Journal of Magnetic Resonance 209 (2011) 269–276

Contents lists available at ScienceDirect

Journal of Magnetic Resonance

journal homepage: www.elsevier.com/locate/jmr

Relaxation dispersion in MRI induced by fictitious magnetic fields

Timo Liimatainen [a,b,*], Silvia Mangia [b], Wen Ling [b], Jutta Ellermann [b], Dennis J. Sorce [b], Michael Garwood [b], Shalom Michaeli [b]

[a] Department of Biotechnology and Molecular Medicine A.I. Virtanen Institute for Molecular Sciences, University of Eastern Finland, Kuopio, Finland
[b] Center for Magnetic Resonance Research and Department of Radiology, University of Minnesota, Minneapolis, USA

ARTICLE INFO

Article history:
Received 3 November 2010
Revised 25 January 2011
Available online 1 February 2011

Keywords:
Relaxation
Rotating frame
Relaxation along fictitious field
Relaxation dispersion
Human brain
Mouse brain

ABSTRACT

A new method entitled Relaxation Along a Fictitious Field (RAFF) was recently introduced for investigating relaxations in rotating frames of rank $\geqslant 2$. RAFF generates a fictitious field (**E**) by applying frequency-swept pulses with *sine* and *cosine* amplitude and frequency modulation operating in a sub-adiabatic regime. In the present work, MRI contrast is created by varying the orientation of **E**, *i.e.* the angle ε between **E** and the z'' axis of the second rotating frame. When $\varepsilon > 45°$, the amplitude of the fictitious field **E** generated during RAFF is significantly larger than the RF field amplitude used for transmitting the *sine*/*cosine* pulses. Relaxation during RAFF was investigated using an invariant-trajectory approach and the Bloch–McConnell formalism. Dipole–dipole interactions between identical (like) spins and anisochronous exchange (*e.g.*, exchange between spins with different chemical shifts) in the fast exchange regime were considered. Experimental verifications were performed *in vivo* in human and mouse brain. Theoretical and experimental results demonstrated that changes in ε induced a dispersion of the relaxation rate constants. The fastest relaxation was achieved at $\varepsilon \approx 56°$, where the averaged contributions from transverse components during the pulse are maximal and the contribution from longitudinal components are minimal. RAFF relaxation dispersion was compared with the relaxation dispersion achieved with off-resonance spin lock $T_{1\rho}$ experiments. As compared with the off-resonance spin lock $T_{1\rho}$ method, a slower rotating frame relaxation rate was observed with RAFF, which under certain experimental conditions is desirable.

1. Introduction

Rotating frame longitudinal and transverse relaxation experiments (with characteristic time constants $T_{1\rho}$ and $T_{2\rho}$, respectively) are capable of probing slow molecular motions at high magnetic fields (B_0) with the motional correlation times in the *ns* to *ms* time scale [1–5]. For some biomedical applications, both $T_{1\rho}$ and $T_{2\rho}$ have been shown to be more informative than laboratory frame T_1 and T_2 in assessing specific tissue pathologic processes, for example cartilage degeneration, gene therapy-induced apoptotic response in BT4C gliomas, cerebral ischemia, and brain iron accumulation and neuronal integrity in patients with Parkinson's disease [6–11]. Although $T_{1\rho}$ and $T_{2\rho}$ measurements are commonly pursued with time-invariant radiofrequency (RF) pulses, these experiments can also be conducted using a train of amplitude – (AM) and frequency-modulated (FM) pulses, each of which completes an adiabatic full-passage (AFP) [12–14].

A potential limitation to the wide spread exploitation of rotating frame relaxation in living systems is the required RF power delivered to the sample (*i.e.*, specific absorption rate (SAR) and concern about tissue heating). To satisfy the adiabatic condition in adiabatic $T_{1\rho}$ and $T_{2\rho}$ experiments, the RF power deposition can sometimes exceed allowable SAR levels for human studies at high magnetic fields. The RF power needed in the classical spin-lock experiments often limits its applicability for human studies, although RF power can sometimes be reduced by using off-resonance irradiation to create the locking field, $\mathbf{B}_{\text{eff}}$ [15]. However, in both on- and off-resonance $T_{1\rho}$ experiments, a separate RF pulse is needed to place the magnetization vector initially at the locking angle, which can be challenging to achieve accurately in the presence of non-uniform RF field ($\mathbf{B}_1$), especially at high magnetic fields.

To satisfy the adiabatic condition, a sufficiently slow frequency sweep must take place to minimize the fictitious field component, $\gamma^{-1}d\alpha/dt\hat{y}$, that exists in a second rotating frame, (the ω_{eff}-frame) where γ is the gyromagnetic ratio and α is the time-dependent angle between the effective RF field $\mathbf{B}_{\text{eff}}$ and the axis of quantization in the first rotating frame, z' (collinear with $\mathbf{B}_0$). By convention $\mathbf{B}_1$ is assumed to be along the x'-axis of the first rotating frame. The

* Corresponding author at: Department of Biotechnology and Molecular Medicine, A.I. Virtanen Institute for Molecular Sciences, University of Eastern Finland, Yliopistonranta 1, 70210 Kuopio, Finland. Tel.: +358 40 355 3903; fax: +358 17 163 030.
E-mail address: timo.liimatainen@uef.fi (T. Liimatainen).

1090-7807/$ - see front matter © 2011 Elsevier Inc. All rights reserved.
doi:10.1016/j.jmr.2011.01.022

vector sum of $\gamma^{-1}d\alpha/dt\hat{y}$ and $\mathbf{B}_{\text{eff}}$ leads to a fictitious effective field $\mathbf{E}$ in the ω_{eff}-frame.

Recently we introduced a rotating frame relaxation experiment that exploits $\mathbf{E}$, called Relaxation Along a Fictitious Field (RAFF). RAFF does not require an initial rotation of the magnetization to a specific locking angle. As compared to continuous wave (CW) $T_{1\rho}$ and adiabatic $T_{1\rho}$ and $T_{2\rho}$ methods, RAFF experiments can be performed with reduced RF power because the stationary spin-locking field $\mathbf{E}$ is produced by AM and FM functions (*sine* and *cosine*, respectively) operating in a sub-adiabatic condition [16]. In the initial RAFF method, we set the angle between $\mathbf{B}_{\text{eff}}$ and $\mathbf{E}$ to $\varepsilon = 45°$ when designing the *sine*/*cosine* pulse, by using parameters satisfying the condition $B_{\text{eff}} = |\gamma^{-1}d\alpha/dt|$. In the present work, we further explore the effect of sub-adiabatic rotation with FM pulses, and use different amplitudes of the fictitious component ($\gamma^{-1}d\alpha/dt$) to produce different locking angles ε and amplitudes of $\mathbf{E}$. With this goal, we first extend the experimental capabilities of the RAFF method, and then use an invariant trajectory method to model the evolution of the transverse and longitudinal components during these *sine*/*cosine* pulses. Finally, we present our initial developments of relaxation theory during RAFF. This theory covers dipolar interactions between like spins in the Redfield limit (fast rotational motion) [17] and anisochronous exchange (*e.g.*, exchange between spins with different chemical shifts) in the fast exchange regime described here using both the invariant-trajectory approach and the Bloch–McConnell formalism. These theoretical efforts are meant to predict general features of the dispersion of relaxation rate constants induced by varying ε in RAFF, while recognizing that they would be inadequate for simulation purposes of intrinsic relaxation parameters of tissue *in vivo*. Based on theoretical predictions and on experimental verifications that we obtained *in vivo* from human and mouse brain, we demonstrate that dispersion of relaxation rates are indeed induced by altering the orientation of $\mathbf{E}$ in the RAFF method, in analogy to how altering the orientation of $\mathbf{B}_{\text{eff}}$ induces dispersion of relaxation rate constants in the CW spin-lock experiment. This property can be utilized to expand the possible MRI contrasts that can be obtained with the RAFF method, thus offering a novel tool to investigate tissues *in vivo* with the sensitivity of rotating frame methods and with acceptable RF power levels. Finally, our results demonstrate that relaxation rate constants are slower with RAFF as compared to conventional off-resonance spin-lock $T_{1\rho}$. This property is especially beneficial at high magnetic fields where relaxation pathways such as anisochronous exchange are significantly accelerated.

2. Theory

2.1. Description of the RAFF method

The ω_{RF}-frame rotates around the laboratory z axis with the time-dependent pulse frequency $\omega_{\text{RF}}(t)$. By convention, the axes of the ω_{RF}-frame are labeled x', y', z'. In this reference frame, the net effective field $\mathbf{B}_{\text{eff}}(t)$ is the vector sum of $B_1(t)\,\hat{\mathbf{x}}'$ and the fictitious field $\gamma^{-1}\Delta\omega(t)\hat{\mathbf{z}}' = \gamma^{-1}(\omega_0 - \omega_{RF}(t))\hat{\mathbf{z}}'$, where $\Delta\omega$ is the offset frequency (*i.e.*, the difference between the Larmor frequency ($\omega_0 = \gamma B_0$) and the pulse frequency (ω_{RF})). The amplitude of $\mathbf{B}_{\text{eff}}(t)$ is given by

$$B_{\text{eff}}(t) = \sqrt{B_1^2(t) + (\gamma^{-1}\Delta\omega(t))^2} \tag{1}$$

and the angle between $\mathbf{B}_{\text{eff}}$ and the first rotating frame z' axis is

$$\alpha(t) = \tan^{-1}\left(\frac{\omega_1(t)}{\Delta\omega(t)}\right) \tag{2}$$

where $\omega_1(t) = \gamma B_1(t)$. When the adiabatic condition, $|\gamma^{-1}d\alpha/dt| \ll B_{\text{eff}}$, is well satisfied, the trajectory of the net magnetization ($\mathbf{M}$) can be approximately described as a simple nutation about $\mathbf{B}_{\text{eff}}(t)$ with the angular velocity $\omega_{\text{eff}}(t) = \gamma B_{\text{eff}}(t)$. In the sub-adiabatic condition, however, the rapid sweep of $\mathbf{B}_{\text{eff}}(t)$ results in a non-negligible fictitious field vector in ω_{eff}-frame (double-primed axis labels, x'', y'', z''). This frame is sometimes referred to as "doubly rotating" because it rotates with frequency $\omega_0 - \omega_{\text{RF}}$ around the z-axis of the laboratory frame and simultaneously with frequency $d\alpha/dt$ around the y'-axis of the ω_{RF}-frame. The magnitude of the fictitious field component that arises from the rotation around the y'-axis is equal to $\gamma^{-1}d\alpha/dt$ and is directed along the y'' axis. Note, y' and y'' axes are collinear, and $\mathbf{B}_{\text{eff}}$ is directed along the z'' axis by convention [16]. The net effective field in the ω_{eff}-frame is therefore the vector sum of $B_{\text{eff}}(t)\,\hat{\mathbf{z}}''$ and $\gamma^{-1}d\alpha/dt\,\hat{\mathbf{y}}''$. Accordingly, the time-dependent amplitude of this net effective field is

$$E(t) = \sqrt{B_{\text{eff}}^2(t) + \left(\gamma^{-1}\frac{d\alpha}{dt}\right)^2} \tag{3}$$

and the angle between $\mathbf{E}$ and $\mathbf{B}_{\text{eff}}$ is

$$\varepsilon(t) = \tan^{-1}\left(\frac{\gamma^{-1}d\alpha/dt}{B_{\text{eff}}(t)}\right) \tag{4}$$

When $B_{\text{eff}}(t)$ and $d\alpha/dt$ are time invariant throughout the pulse, the amplitude of $\mathbf{E}$ remains constant. From Eq. (4), it can be seen that a change of $\gamma^{-1}d\alpha/dt$ relative to $B_{\text{eff}}(t)$ creates the possibility to vary the locking angle ε. It can also be seen that the magnitude of $\mathbf{E}$ is greater than the peak RF amplitude, $B_1^{\max} = \gamma^{-1}\omega_1^{\max}$ (Fig. 1, and Eq. (3)).

In our prior work, $\mathbf{E}$ was kept stationary with $\varepsilon = 45°$ by choosing AM and FM shapes based on *sine* and *cosine* functions with equal amplitudes [16]. However, the angular velocity of the sweep ($d\alpha/dt$) depends on the arguments of the *sine* and *cosine* functions. It is straightforward to verify that a stationary angle ε of any arbitrary value can be produced. To accomplish this, let us modulate the pulse amplitude and offset frequency according to *sine* and *cosine* functions having maximum amplitude of ω_1^{max} and frequency ω,

$$\omega_1(t) = \omega_1^{\max}\sin(\omega t) \tag{5}$$

$$\Delta\omega(t) = \omega_1^{\max}\cos(\omega t) \tag{6}$$

In this case, the amplitude of $\mathbf{B}_{\text{eff}}(t)$ can be simplified based on Eq. (1) to

$$\begin{aligned} B_{\text{eff}}(t) &= \sqrt{(\gamma^{-1}\omega_1^{\max}\sin(\omega t))^2 + (\gamma^{-1}\omega_1^{\max}\cos(\omega t))^2} \\ &= \gamma^{-1}\omega_1^{\max} \end{aligned} \tag{7}$$

This result, when combined with Eq. (4), leads to

$$\frac{d\alpha(t)}{dt} = \omega_1^{\max}\tan(\varepsilon(t)) \tag{8}$$

It can be verified using Eqs. (2), (5), and (6) that, to produce a given angle ε, ω must equal $d\alpha/dt$. That is,

$$\begin{aligned} \frac{d\alpha(t)}{dt} &= \frac{d}{dt}\tan^{-1}\left(\frac{\omega_1^{\max}\sin(\omega t)}{\omega_1^{\max}\cos(\omega t)}\right) = \frac{d}{dt}\tan^{-1}(\tan(\omega t)) \\ &= \frac{d}{dt}\omega t = \omega \end{aligned} \tag{9}$$

Therefore, the amplitude and frequency modulation functions based on Eqs. (5), (6), (8), and (9) are

$$\omega_1(t) = \omega_1^{\max}\sin\left(\omega_1^{\max}\tan(\varepsilon)t\right) \tag{10}$$

$$\Delta\omega(t) = \omega_1^{\max}\cos\left(\omega_1^{\max}\tan(\varepsilon)t\right) \tag{11}$$

The analytical form for the phase modulation function of the pulse, which is typically applied in the MR scanners, can be obtained by

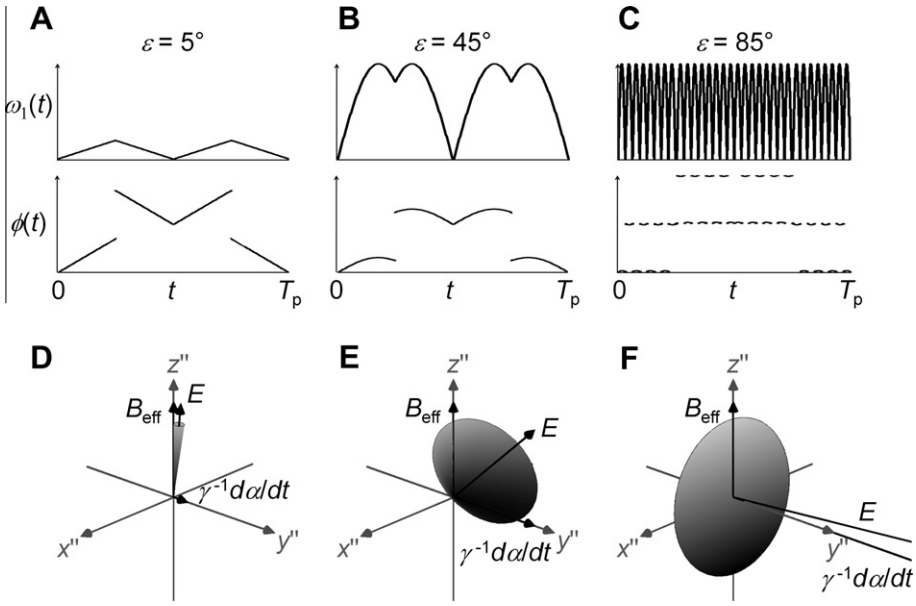

Fig. 1. RF pulse amplitude ($\omega_1(t)$) and phase ($\phi(t)$) modulation functions corresponding to $\varepsilon = 5°$ (A), $\varepsilon = 45°$ (B), $\varepsilon = 85°$ (C) with the refocusing scheme during RAFF; and planes of magnetization rotation for initial magnetization along z'' ($\mathbf{M}(t = 0) = [0\ 0\ 1]$) (D–F) are shown. Note, the scales of $\omega_1(t)$ and $\phi(t)$ are equally scaled for separate ε.

$$\phi(t) = \int_0^t \Delta\omega(t')dt' \tag{12}$$

Substitution of the frequency offset function given by Eq. (11) into Eq. (12) yields the *sine*/*cosine* phase modulation function of the pulse,

$$\phi(t) = \frac{1}{\tan(\varepsilon)} \sin\left(\omega_1^{\max} \tan(\varepsilon) t\right) \tag{13}$$

In this work, the RAFF pulse was calculated using Eqs. (5) and (6), and the length of each RAFF pulse element was chosen as

$$T_p = \frac{4\pi}{\sqrt{2}\omega_1^{\max}} \tag{14}$$

for all angles of ε used. In experiments and simulations, the basic RAFF pulse element to produce a specified ε was concatenated to create a set of windowless RAFF trains. Examples of the basic RAFF pulse element ($\varepsilon = 5°$, 45°, and 85°) are shown in Fig. 1. In previous work [16], a phase of $\pi\left(\sqrt{2}-1\right)$ was added to the middle section of the RAFF element to achieve self-refocusing, as used in the adiabatic plane rotation pulse, BIR-4 [18]. For an arbitrary choice of the time-invariant parameter ε, the RAFF modulation functions, including self-refocusing, are:

$$\begin{aligned}
\omega_1(t) &= \omega_1^{\max} \sin\left(\omega_1^{\max} \tan(\varepsilon) t\right) \quad 0 \leqslant t < T_p/4 \\
\phi(t) &= \frac{1}{\tan(\varepsilon)} \sin\left(\omega_1^{\max} \tan(\varepsilon) t\right) \quad 0 \leqslant t < T_p/4 \\
\omega_1(t) &= \omega_1^{\max} \sin\left(\omega_1^{\max} \tan(\varepsilon)\left(t - \frac{T_p}{2}\right) + \pi\right) \quad T_p/4 \leqslant t < T_p/2 \\
\phi(t) &= \frac{1}{\tan(\varepsilon)} \sin\left(\omega_1^{\max} \tan(\varepsilon)\left(t - \frac{T_p}{2}\right) + \pi\right) \quad T_p/4 \leqslant t < T_p/2 \\
\omega_1(t) &= \omega_1^{\max} \sin\left(\omega_1^{\max} \tan(\varepsilon)\left(t - \frac{T_p}{2}\right)\right) \quad T_p/2 \leqslant t < 3/4T_p \\
\phi(t) &= \frac{1}{\tan(\varepsilon)} \sin\left(\omega_1^{\max} \tan(\varepsilon)\left(t - \frac{T_p}{2}\right)\right) \quad T_p/2 \leqslant t < 3/4T_p \\
\omega_1(t) &= \omega_1^{\max} \sin\left(\omega_1^{\max} \tan(\varepsilon)(t - T_p) + \pi\right) \quad 3/4T_p \leqslant t \leqslant T_p \\
\phi(t) &= \frac{1}{\tan(\varepsilon)} \sin\left(\omega_1^{\max} \tan(\varepsilon)(t - T_p) + \pi\right) \quad 3/4T_p \leqslant t \leqslant T_p
\end{aligned} \tag{15}$$

An additional phase of π must be added to the phase function during the times when the amplitude modulation function is negative (*i.e.*, a π phase shift is the equivalent of a change in sign of $\omega_1(t)$). Notably, the period of the *sine* and *cosine* functions is longer than the RAFF pulse element when $(\omega_1(t)\tan(\varepsilon))^{-1} \geqslant T_p/4$; in this case, the amplitude of the RAFF pulse element does not reach $\omega_1^{\max}$ with $\varepsilon < 24°$ (Fig. 1).

If **M** is initially aligned with $\mathbf{B}_{\text{eff}}$, during the RAFF pulse it precesses on a cone having an axis defined by the vector **E**. Wigner rotation matrices can be used to transform from the ω_{RF}-frame (x', y', z') to the ω_{eff}-frame (x'', y'', z''), followed by a final rotation around x'' by the angle ε to align the axis of quantization (z'') along **E**.

2.2. Invariant trajectory

When the spin rotation is characterized by rotational correlation times on the order of *ps*/*ns*, the Redfield relaxation theory (or fast motion limit) with the perturbation treatment of the spin dynamics applies because the corresponding relaxation rate constants are larger than the NMR anisotropies (in frequency units) modulated by the rotational motion [2,17,19]. Here, the condition applicable to non-viscous liquids should be satisfied, $\omega_{\text{eff}}\tau_c \ll 1$. The invariant-trajectory approach introduced by Griesinger and Ernst [20] can be used to calculate the relaxation rate constants in the presence of RF irradiation. For dipolar auto-relaxations of like spins, the effective relaxation rate constant R^{eff} is given by:

$$\begin{aligned}
R^{\text{eff}} &= R_2 \frac{1}{T_p} \int_0^{T_p} \{M_x(t)^2 + M_y(t)^2\} dt + R_1 \frac{1}{T_p} \int_0^{T_p} (M_z(t)^2 dt \\
&= R_2 \cdot C_{\text{tr}} + R_1 \cdot C_{\text{long}},
\end{aligned} \tag{16}$$

where R_1 and R_2 are free precession longitudinal and transverse relaxation rate constants respectively, while C_{long} and C_{tr} represent their relative weightings and the integration is over the duration of the pulse of T_p. The weighted average depends on the trajectory of the normalized magnetization vector $\mathbf{M}(t) = [M_x(t), M_y(t), M_z(t)]$, with the condition

$$C_{tr} + C_{\text{long}} = 1 \tag{17}$$

being satisfied. Similar equations have been found for evaluating exchange-induced relaxation rate constants when setting R_2 and R_1 in Eq. (16) to

$$\begin{aligned} R_2 &= P_A P_B \delta\omega^2 \tau_{ex} \\ R_{1,\mathrm{ex}} &= 0 \end{aligned} \tag{18}$$

As will be shown below, this approach agrees well with the Bloch–McConnell treatment.

2.3. Evaluating exchange-induced relaxations using invariant-trajectory approach

In order to use the invariant-trajectory approach to calculate relaxation rate constants in RAFF, the magnetization trajectory during RAFF irradiation needs to be calculated. The generalized matrix describing rotation around an arbitrary axis in three-dimensional space is given by normalized unit vectors $[u, v, w]$ which has the form

$$\Re(\varphi) = \begin{bmatrix} u^2 + (v^2+w^2)\cos(\varphi) & uv(1-\cos(\varphi)) - w\sqrt{u^2+v^2+w^2}\sin(\varphi) & uv(1-\cos(\varphi)) + v\sqrt{u^2+v^2+w^2}\sin(\varphi) \\ uv(1-\cos(\varphi)) + w\sqrt{u^2+v^2+w^2}\sin(\varphi) & v^2 + (u^2+w^2)\cos(\varphi) & vw(1-\cos(\varphi)) - u\sqrt{u^2+v^2+w^2}\sin(\varphi) \\ uw(1-\cos(\varphi)) - v\sqrt{u^2+v^2+w^2}\sin(\varphi) & vw(1-\cos(\varphi)) + u\sqrt{u^2+v^2+w^2}\sin(\varphi) & w^2 + (u^2+v^2)\cos(\varphi) \end{bmatrix} \tag{19}$$

for time invariant angle φ. In the ω_{eff}-frame, the amplitude of **E** in rad/s is ω_E, so the angle of rotation of **M** at time t is $\omega_E t$ and the direction of **M** is defined by the normalized unit vectors $[u = 0, v = \sin(\varepsilon), w = \cos(\varepsilon)]$. It is noticed here that ε is time invariant. When viewing from the ω_{eff}-frame, **M** initially aligned along z'' will evolve according to:

$$\mathbf{M}(t) = \Re(\omega_E t) M_0 = \Re(\omega_E t) \begin{bmatrix} 0 \\ 0 \\ 1 \end{bmatrix} = \begin{bmatrix} \sin(\varepsilon)\sin(\omega_E t) \\ \sin(\varepsilon)\cos(\varepsilon)(1-\cos(\omega_E t)) \\ \cos^2(\varepsilon) + \sin^2(\varepsilon)\cos(\omega_E t) \end{bmatrix} \tag{20}$$

Transformation from the ω_{eff}-frame to the ω_{RF}-frame is performed around y' axis with the rotation matrix given by:

$$\Re(\alpha(t)) = \begin{bmatrix} \cos(\alpha(t)) & 0 & \sin(\alpha(t)) \\ 0 & 1 & 0 \\ -\sin(\alpha(t)) & 0 & \cos(\alpha(t)) \end{bmatrix} \tag{21}$$

Thus, the magnetization trajectory in the ω_{RF}-frame is described as:

$$M'(t) = \Re(\alpha(t))\Re(\omega_E(t)t)M_0 = \Re(\alpha(t))M(t) = \begin{bmatrix} \cos(\alpha(t))\sin(\varepsilon(t))\sin(\omega_E(t)t) + \sin(\alpha(t))(\cos^2(\varepsilon(t)) + \sin^2(\varepsilon(t))\cos(\omega_E(t)t)) \\ \sin(\varepsilon(t))\cos(\varepsilon(t))(1-\cos(\omega_E(t)t)) \\ -\sin(\alpha(t))\sin(\varepsilon(t))\sin(\omega_E t) + \cos(\alpha(t))(\cos^2(\varepsilon(t)) + \sin^2(\varepsilon(t))\cos(\omega_E(t)t)) \end{bmatrix} \tag{22}$$

Now, the $M_x(t)$ and $M_y(t)$ components of $\mathbf{M}(t)$ are given by:

$$\begin{aligned} M_x(t) &= \cos(\alpha(t))\sin(\varepsilon(t))\sin(\omega_E(t)t) + \sin(\alpha(t))(\cos^2(\varepsilon(t)) \\ &\quad + \sin^2(\varepsilon(t))\cos(\omega_E(t)t)) \\ M_y(t) &= \sin(\varepsilon(t))\cos(\varepsilon(t))(1-\cos(\omega_E(t)t)) \end{aligned} \tag{23}$$

Here, $\alpha(t) = \tan(\varepsilon)\omega_1^{\max} t$. Finally, substituting Eq. (18) in Eq. (16) the exchange-induced relaxation rate constant R_{RAFF}^{ex} in the case of two-site anisochronous exchange (2SX) in the fast exchange regime is

$$R_{\mathrm{RAFF}}^{ex} = P_a P_b \delta\omega^2 \tau_{ex} \left(\frac{1}{T_p} \int_0^{T_p} \left(M(t)_x^2 + M(t)_y^2 \right) dt \right) \tag{24}$$

with $M_x(t)$ and $M_y(t)$ given by Eq. (23). Here, P_A and P_B are populations of exchanging sites A and B with chemical shift difference $\delta\omega$ in rad/s and exchange correlation time τ_{ex}. It should be noted that the consideration above is valid for like spin at one specific sites A or B.

2.4. Bloch–McConnell formulation of the relaxations during RAFF

Relaxations during RF irradiation due to dipolar interactions (like spins) and induced by anisochronous exchange between two pools A and B can be described using Bloch–McConnell equations written in the phase-modulated rotating frame [21]:

$$\begin{aligned} \frac{dM_z^A(t)}{dt} &= \frac{M_0^A - M_z^A(t)}{T_{1A}} - k_{\mathrm{ex}}^{AB} M_z^A(t) + k_{\mathrm{ex}}^{BA} M_z^B(t) + \omega_1 \sin(\phi) M_x^A(t) - \omega_1 \cos(\phi) M_y^A(t) \\ \frac{dM_z^B(t)}{dt} &= \frac{M_0^B - M_z^B(t)}{T_{1B}} - k_{\mathrm{ex}}^{BA} M_z^B(t) + k_{\mathrm{ex}}^{AB} M_z^A(t) + \omega_1 \sin(\phi) M_x^B(t) - \omega_1 \cos(\phi) M_y^B(t) \\ \frac{dM_x^A(t)}{dt} &= -\frac{M_x^A(t)}{T_{2A}} - k_{\mathrm{ex}}^{AB} M_x^A(t) + k_{\mathrm{ex}}^{BA} M_x^B(t) - \Delta_A M_y^A(t) - \omega_1 \sin(\phi) M_z^A(t) \\ \frac{dM_x^B(t)}{dt} &= -\frac{M_x^B(t)}{T_{2B}} - k_{\mathrm{ex}}^{BA} M_x^B(t) + k_{\mathrm{ex}}^{AB} M_x^A(t) - \Delta_B M_y^B(t) - \omega_1 \sin(\phi) M_z^A(t) \\ \frac{dM_y^A(t)}{dt} &= -\frac{M_y^A(t)}{T_{2A}} - k_{\mathrm{ex}}^{BA} M_y^B(t) + k_{\mathrm{ex}}^{AB} M_y^A(t) + \Delta_A M_x^A(t) + \omega_1 \cos(\phi) M_z^A(t) \\ \frac{dM_y^B(t)}{dt} &= -\frac{M_y^B(t)}{T_{2B}} - k_{\mathrm{ex}}^{BA} M_y^B(t) + k_{\mathrm{ex}}^{AB} M_y^A(t) + \Delta_B M_x^B(t) + \omega_1 \cos(\phi) M_z^B(t) \end{aligned} \tag{25}$$

where $\Delta_{A,B}$ are the chemical shifts relative to on-resonance in rad/s of exchanging groups A and B, respectively ($\delta\omega = |\Delta_A + \Delta_B|$), P_A and P_B are the populations of the exchanging sites, $k_{\mathrm{ex}}^{AB} = P_B/\tau_{\mathrm{ex}}$ and $k_{\mathrm{ex}}^{BA} = P_A/\tau_{\mathrm{ex}}$ are the exchange rate constants, and $T_{1,2,A,B} = 1/R_{1,2,A,B}$ are the relaxation time constants at sites A and B, respectively. Here, the *sine*/*cosine* modulation functions (Eq. (15)) were used. The RF pulse amplitude was set to $\omega_1^{\max}/(2\pi) = 625$ Hz and the pulse duration (T_p) was set according to Eq. (14). For the simulations, 15 linearly spaced angles ε between 5° and 85° were generated. The pulse train was extended by increasing the number of basic RAFF elements up to a total length of 144.82 ms. The R_1 and R_2 were

calculated considering dipolar interactions between isolated identical spins (at specific sites A and B), following:

$$R_1 = \frac{3}{10} b^2 \left(\frac{\tau_c}{1+\tau_c^2\omega_0^2} + 4\frac{\tau_c}{1+4\tau_c^2\omega_0^2} \right) \quad (26)$$

and

$$R_2 = \frac{3}{20} b^2 \left(3\tau_c + \frac{5\tau_c}{1+\tau_c^2\omega_0^2} + \frac{2\tau_c}{1+4\tau_c^2\omega_0^2} \right) \quad (27)$$

where τ_c is the rotational correlation time and ω_0 is the Larmor precession frequency, $b = -\mu_0\hbar\gamma^2/(4\pi r^3)$, $\mu_0 = 4\pi \times 10^{-7}$ H/m is the vacuum permeability, $\hbar = 1.055 \times 10^{-34}$ Js is Planck's constant, and r is the internuclear distance in meters. The dipolar interaction theory used in this work is an over-simplification for biologic tissues, where a variety of dipolar mechanisms contribute to relaxation. However, the complete description of dipolar relaxation is outside of the scope of this work. The simulations of the two-site exchange were carried out using Eq. (24) with T_1 and T_2 calculated using $\tau_c = 2 \times 10^{-12}$ s for both sites A and B. The decay of $\mathbf{M}$ ($\mathbf{M}_0 = [0\ 0\ 1]$) during the pulse was estimated by solving Eq. (25) using the Runge–Kutta numerical method. Simulations were performed with magnetization initially oriented along z' $\mathbf{M}_0 = [0\ 0\ 1]$ and then for inverted $\mathbf{M}_0 = [0\ 0\ -1]$ to include the steady state in the analysis. The approach of placing magnetization initially along the $+z$ or $-z$ axis was previously described in detail [16], and was shown to facilitate the analysis of the relaxations during *sine* / *cosine* pulses.

3. Materials and methods

All human experiments were performed according to procedures approved by the Institutional Review Board of the University of Minnesota Medical School. After obtaining informed consent, MRI measurements on human brain (of five healthy volunteers) were performed with a 4 T magnet (Oxford Instruments) interfaced to a Varian ^{UNITY}INOVA console. A volume coil based on the transverse electromagnetic design was utilized for brain imaging [22]. Images were acquired using fast spin echo readout, TR = 4.5 s, 15 ms echo spacing, number of echoes 8, matrix size 256 × 128, FOV = 256 × 256 mm^2, and slice-thickness = 4 mm. Maps of the RAFF relaxation rate constant (R_{RAFF}) were generated with 0, 36, 72, 108, 144 ms preparation pulse train lengths. *Sine*/*cosine* pulse power calibration was performed using LASER localization [23] in voxels placed in the area of interest and using 400 μs hard pulse to be calibrated as 90° excitation.

A total of three c57bl mice from the University of Eastern Finland, National Laboratory Animal Center, Finland were imaged in this study. The mice were housed in a controlled environment with free access to food and water. Animal experiments were reviewed and approved by the national Animal Experiment Board and conducted in accordance with the guidelines set by the European Community Council Directives 86/609/EEC. Mice were scanned in a 9.4 T vertical magnet (Oxford Instruments, Plc., Witney, UK) interfaced to a Varian DirectDrive console. A quadrature volume transceiver coil (diameter 23 mm) (Rapid Biomedical GmbH, Rimpar, Germany) was used for mouse brain imaging. In all experiments, anesthesia was induced using 4.5% and maintained with 1.5% isoflurane during the experiment in oxygen/N_2O with fractions 0.21:0.79. Temperatures of animals were maintained using a circulating water heater. For off-resonance CW $T_{1\rho}$, spin lock durations between 20 and 120 ms (four values linearly spaced) were selected with hard pulse excitation and 180° phase flip in the middle of the CW pulse. Pulse durations were selected similarly for RAFF but linearly spaced up to 144 ms. For both setups, $\gamma B_1/(2\pi)$ = 625 Hz (also for hard pulse excitation). For RAFF, a standard hyperbolic secant pulse (HS1), with T_p = 4 ms, time-bandwidth product (R) = 10, and peak amplitude = 2.5 kHz, was used for initial inversion to allow steady state fitting. A fast spin-echo sequence was used for readout with TR = 4 s, effective TE = 6.85 ms, echo spacing 3.3 ms, number of echoes in the pulse train = 4, field-of-view = 19.2 × 19.2 mm^2, and matrix size = 128 × 128 for readout.

Experimental details of the acquisition strategy used for obtaining RAFF maps were described in detail in [16]. Briefly, signal intensity decay and rise during *sine*/*cosine* pulses for the different angles of RAFF were collected consequently with and without initial inversion of magnetization. The results with and without initial inversion of magnetization were simultaneously fitted using model that takes into account the formation of a steady state [16]

$$S_{\pm Z}(t) = S_{0,\pm Z} e^{-R_{RAFF}t} - S_{SS}(1 - e^{-R_{RAFF}t}) \quad (28)$$

in which $S_{0,\pm Z}$ are the initial amplitudes of magnetization before the application of *sine*/*cosine* pulse (with and without inversion), and S_{SS} is the amplitude of magnetization when the pulse train length approaches infinity. Relaxation maps were generated pixel-wise using Matlab 7.1 (Mathworks Inc., Natick, MA, USA).

4. Results and discussion

During the *sine*/*cosine* pulse, $\mathbf{M}$ undergoes precession around $\mathbf{E}$ in the second rotating frame (the ω_{eff}-frame) (Figs. 1 and 2). Using Bloch simulations we demonstrated previously that $\mathbf{E}$ behaves as a spin-locking field [16]. A unique feature of the RAFF method is that the amplitude of $\mathbf{E}$ can be larger than the input RF amplitude used for the *sine*/*cosine* pulses (Eqs. (1)–(3)), and the amplitude of $\mathbf{E}$ approaches its maximal value with $\varepsilon \to 90°$. Thus, RAFF might be exploited in rotating frame relaxation experiments to achieve a large spin-lock field without increasing the RF amplitude.

In Fig. 2, the trajectories of $\mathbf{M}$ in the first rotating frame (the ω_{RF}-frame) are presented. The simulations were performed using the Runge–Kutta algorithm to solve the Bloch equations. The trajectories of $\mathbf{M}$ for a given ε between 5° and 85° demonstrate that $\mathbf{M}$ nutates only slightly from z' axis when ε is small and large. With small ε, $\mathbf{M}$ undergoes slow nutation to a small angle. On the other hand, with large values of ε (when $\varepsilon \to 90°$), fast oscillations of both frequency and amplitude modulations occur (see Eqs. (5) and (6)). For large angles, $\mathbf{E}$ is close to y'', and in the second rotating frame, $\mathbf{M}$ precesses in the plane almost perpendicular to $\mathbf{E}$ with increasing

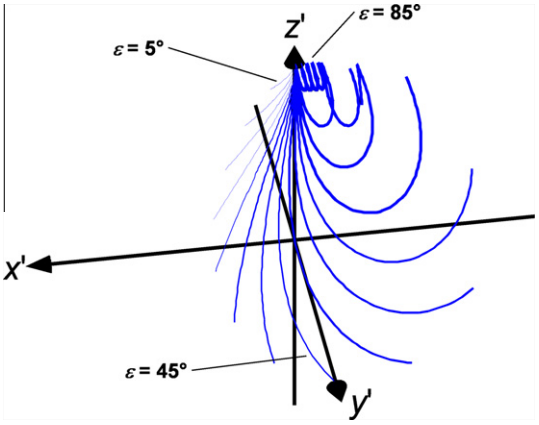

Fig. 2. Magnetization trajectories during the first segments of *sine*/*cosine* pulses with different ε angles are shown. Fifteen ε values were evenly distributed between 5° and 85°, and the RF pulse amplitude and frequency modulation functions generated with $\omega_1^{max}/(2\pi) = 625$ Hz were used. The Runge–Kutta algorithm was used for simulating the Bloch equations.

number of the trajectory cycles as ε increases**.** The latter phenomenon becomes evident especially with high values of ε. The number of these cycles depends on how close **E** is to y'', or equivalently, how fast $\mathbf{B}_{\text{eff}}$ rotates relative to z'. Despite the high amplitude of the effective field, the effective tip angle of **M** may remain small due to the rapid change in the direction of **E** in the ω_{RF}-frame. For intermediate values of ε, **M** nutates with larger angles.

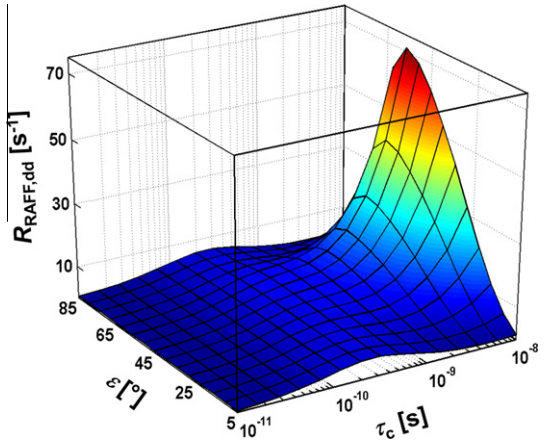

Fig. 3. Simulated relaxation rate constants due to dipolar interactions ($R_{\text{RAFF,dd}}$) between two identical spins as a function of angle ε and correlation time τ_c. For the simulations, Eq. (28) was used under the condition $k_{AB}^{ex} = 0$, along with Eqs. (29) and (30). $\tau_c = 2 \times 10^{-12}$ s was assumed for both sites *A* and *B*. $\omega_1^{\max}/(2\pi) = 625$ Hz.

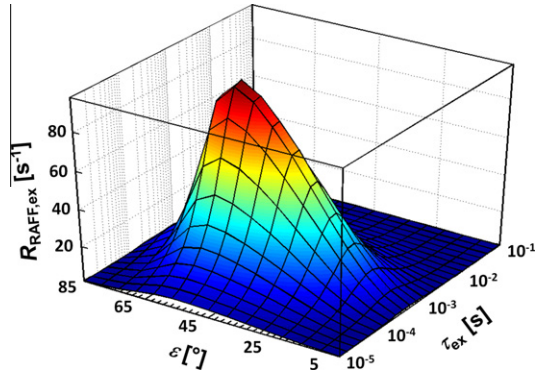

Fig. 4. Simulated exchange-induced relaxation rate constants ($R_{\text{RAFF,ex}}$) between spins with different chemical shifts as a functions of ε and exchange correlation times (τ_{ex}). For the simulations, Eqs. (28), (29) and (30) were used. For both sites *A* and *B*, $\tau_c = 2 \times 10^{-12}$ s was assumed. Other assumptions: difference in chemical shifts, $\delta\omega = 0.85$ ppm; $P_A = P_B = 0.5$; $\omega_1^{\max}/(2\pi) = 625$ Hz.

Results of calculations of the relaxation rate constant due to dipolar interactions between like spins ($R_{\text{RAFF,dd}}$) are presented in Fig. 3. This analysis of RAFF was performed using the Bloch equations. It can be seen that when $T_1 \approx T_2$, which corresponds to rotational correlation times shorter than 5×10^{-10} s, $R_{\text{RAFF,dd}}$ is independent of the angle ε. With longer correlation times, when $T_1 \neq T_2$, a significant dependence of R_{RAFF} on ε was found. The greatest R_{RAFF} values were observed for angles ε ranging between 50° and 60°.

The simulations of the exchange-induced relaxation rate constant ($R_{\text{RAFF,ex}}$) were performed using Bloch–McConnell formalism for two-site equilibrium exchange Eq. (24). In Fig. 4, it is shown that, for small $\tau_{\text{ex}} < 10^{-5}$ s and large $\tau_{\text{ex}} > 10^{-2}$ s, $R_{\text{RAFF,ex}}$ values are independent of ε. This property of $R_{\text{RAFF,ex}}$ is similar to the $R_{\text{RAFF,dd}}$ dependence on ε for the correlation times $\tau_c \geqslant 10^{-9}$ s (Fig. 4). In the intermediate region of correlation times, $R_{\text{RAFF,ex}}$ attains its maximum at $\varepsilon = 56°$.

The relative weighting contributions of the magnetization components during RAFF were investigated using invariant-trajectory approach Eqs. (16)–(24). In Fig. 5a, the integrated magnetization weighting, *i.e.*, normalized coefficients of transverse, C_{tr}, and longitudinal, C_{long}, components Eq. (18) are shown. It can be seen that the maximal weighting of transverse magnetization occurs with $\varepsilon = 56°$ where the contribution of the longitudinal magnetization weighting is minimal. On the other hand, with the smaller and larger ε the contribution of M_z becomes greater and the contribution of M_x and M_y reduce. This suggests that largest R_{RAFF} should be detected when $\varepsilon = 56°$. The calculation of the R_{RAFF} rate constants were performed using Eqs. (19)–(24) for invariant trajectory and for Bloch–McConnell approaches Eq. (25). Evidently, when **M** spends more time close to the *xy*-plane the values of R_{RAFF} are greater (Fig. 5a). It can be seen in Fig. 4 and in Fig. 5B that these two methods correspond well and closely describe exchange-induced relaxation rate constants dependencies on the angle ε.

In Fig. 6A–C, a representative example of the human brain relaxation mapping with RAFF from one healthy subject at 4*T* is presented along with the anatomic image in Fig. 6D. The multi-subject ($n = 5$) averaged rate constants from the ROIs indicated in Fig. 6D from substantia nigra (SN) and CSF areas are shown in Fig. 6E. The rate constants measured with RAFF (R_{RAFF}) are

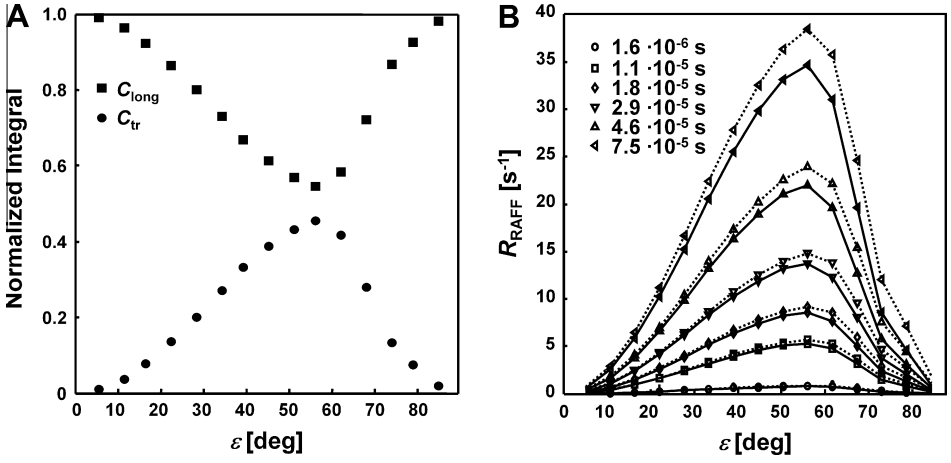

Fig. 5. (A) Magnetization weighting coefficients C_{tr} and C_{long} Eqs. (20), (21) averaged over time during the RAFF pulse, plotted as a function of ε. B) Theoretical simulations of exchange-induced relaxations with RAFF using Bloch–McConnell formalism Eqs. (25)–(27) (dashed line) and invariant trajectory method Eq. (24) (solid line), as a function of ε for different exchange–correlation times. For both sites *A* and *B*, $\tau_c = 2 \times 10^{-12}$ s was assumed. Other parameters: difference in chemical shifts, $\delta\omega = 0.85$ ppm; $P_A = P_B = 0.5$; $\omega_1^{\max}/(2\pi) = 625$ Hz. Exchange correlation times are shown in the inset of (B).

significantly dependent on ε as can be seen in Fig. 6E. Here, a superior difference in R_{RAFF}, greater than double, between the measurements with RAFF at 56° and 74° was detected. The differences in tissue R_{RAFF} values obtained with small and large εs are significantly bigger than those in CSF (almost no difference), suggesting good sensitivity of RAFF to slow dynamics in tissues. The results of the RAFF measurements in mouse cortex are shown in Fig. 7. Here, the comparison with CW spin lock $T_{1\rho}$ was also performed at 9.4 T, and the dependencies on angles ε (for RAFF) and α (for CW $T_{1\rho}$) were investigated. It can be seen that with RAFF the maximum rate constant is observed at $\varepsilon = 56°$. As expected with CW $T_{1\rho}$, the maximum rate constant is measured at $\alpha = 90°$ since $T_{1\rho} \rightarrow T_2$ in the Redfield limit (fast motional regime) [17]. This experiment demonstrates an advantage of RAFF as compared to conventional CW $T_{1\rho}$ for rotating frame relaxation measurements at high magnetic fields (3*T* and above), where the relaxations induced by exchange and diffusion in local magnetic gradients (collectively referred to here as dynamic averaging) are

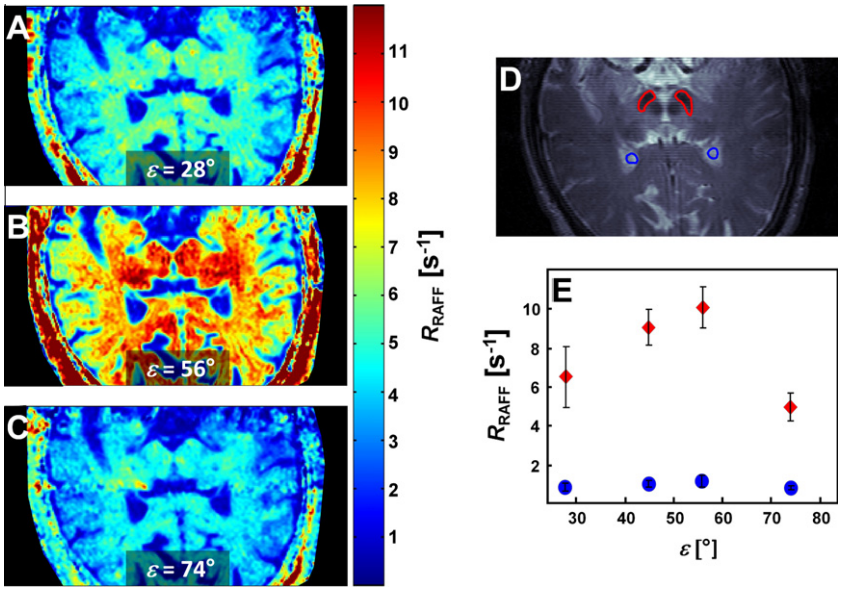

Fig. 6. Maps of the relaxation rate constant R_{RAFF} obtained from the human brain of one representative volunteer at 4 T when using *sine*/*cosine* pulses with different ε angles: (A) 28°, (B) 56° and (C) 74°. T_2 weighted anatomic reference image (D) and multi-subject averaged relaxation rate constants (E) from regions of interest (red and green in D represent gray matter and CSF, respectively), plotted as a function of ε. Data are presented as mean ± SD ($n = 5$ for all angles except $\varepsilon = 45°$ where number of studies $n = 4$).

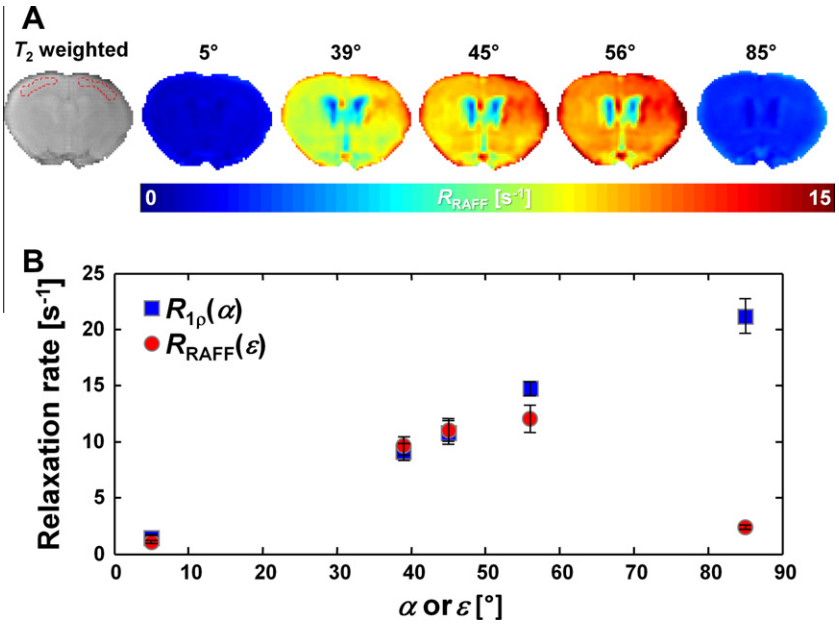

Fig. 7. (A) Maps of the relaxation rate constant (R_{RAFF}) measured in the intact mouse brain using several settings of the locking angle ε. Also shown is a T_2-weighted anatomic image of the same slice with the ROIs used for the analysis. The differences in the RAFF 45° rate constants between right and left hemispheres of the brain was found on average to be 6.3% ($n = 3$) and the displayed are the averaged rate constants between both sides of the brain. (B) A comparison between R_{RAFF} and CW off-resonance $R_{1\rho}$. The mean ± SD values are shown ($n = 3$).

significantly accelerated. This is particularly important for probing slow motional correlation times when the relaxation rates could be so large that the signal escapes detection.

Our theoretical description, although performed using the most parsimonious relaxation models, well described our *in vivo* results. At this stage of investigation we did not intend to describe the details of specific relaxation pathways during RAFF in the human brain, for example, relaxations due to dipolar interactions, dynamic averaging (*e.g.*, anisochronous/isochronous mechanisms), residual dipolar interactions, or cross relaxations. Detailed theoretical treatments are necessary to completely understand the relaxation during RAFF *in vivo*. The developed RAFF method provides a possibility to generate novel contrast in MR which is based on the relaxations in the presence of the fictitious field **E**. Based on the theoretical and experimental results presented in this work, the RAFF method provides excellent sensitivity to spin dynamics since it comprises characteristics of both rotating frame relaxation methods, $T_{1\rho}$ and $T_{2\rho}$. In addition, due to its highly efficient refocusing properties, the RAFF method has similarities to the Carr–Purcell–Meiboom–Gill (CPMG) method [24], while simultaneously having characteristics of the classical rotating frame rotary echo technique [5]. Due to its sensitivity to different relaxation channels *in vivo* particularly in the slow motional regime, MRI contrast based on RAFF has potential utility for a number of *in vivo* applications.

5. Conclusions

Here, we presented a method to create relaxation dispersion using a (partially) fictitious field **E** and altering its magnitude and orientation, in a doubly rotating frame of reference. The amplitude of **E** can be greater than the RF amplitude used in transmitting RAFF pulses and thus provides an alternative means to increase the magnitude of the spin-lock field without increasing the RF power. In the presence of dipolar interactions and exchange–induced relaxation between spins with different chemical shifts, the relaxation rate during RAFF has a large dependence on the tilt angle ε of the fictitious field **E**. Maximum values of R_{RAFF} were shown to occur at $\varepsilon = 56^{\circ}$, which is consistent with the weighted contributions to the relaxations from transverse and longitudinal magnetization components using an invariant trajectory analysis and Bloch–McConnell formalism. The RAFF method comprises properties of the second rotating frame relaxation method with sensitivity to slow motion and efficient refocusing of the rotating frame rotary echo, and thus holds potential to generate unique contrast for MRI. With RAFF, relaxation rates are slower than with conventional off-resonance spin-lock $T_{1\rho}$. This suggest its applicability for the rotating frame relaxation measurements at high magnetic fields (3*T* and above) where the relaxations induced by dynamic averaging are accelerated.

Acknowledgments

The authors the following agencies for financial support: Instrumentarium Science Foundation (TL), Orion Corporation Research Foundation (TL), Finnish Cultural Foundation Northern Savo (TL), and NIH grants P30 NS057091, P41 RR008079, R01 NS061866, and R21 NS059813.

References

[1] D. Abergel, A. Palmer III, On the use of the stochastic Liouville equation in nuclear magnetic resonance: application to $R_{1\rho}$ relaxation in the presence of exchange, Concept. Magn. Reson. A 19 (2003) 134–148.
[2] A. Abragam, Principles of Nuclear Magnetism, Oxford University Press Inc., Oxford, 1963. pp. 517–522.
[3] M. Fischer, A. Majumdar, E. Zuiderweg, Protein NMR relaxation: theory, applications and outlook, Prog. NMR Spectrosc. 33 (1998) 207–272.
[4] A. Palmer, C. Kroenke, J. Loria, Nuclear magnetic resonance methods for quantifying microsecond-to-millisecond motions in biological macromolecules, Method Enzymol. 339 (2001) 204–238.
[5] I. Solomon, Rotary spin echoes, Phys. Rev. Lett. 2 (1959) 301–305.
[6] A. Borthakur, E. Mellon, S. Niyogi, W. Witschey, J.B. Kneeland, R. Reddy, Sodium and $T_{1\rho}$ MRI for molecular and diagnostic imaging of articular cartilage, NMR Biomed. 19 (2006) 781–821.
[7] H.I. Gröhn, S. Michaeli, M. Garwood, R.A. Kauppinen, O.H. Gröhn, Quantitative $T_{1\rho}$ and adiabatic Carr–Purcell T_2 magnetic resonance imaging of human occipital lobe at 4 T, Magn. Reson. Med. 54 (2005) 14–19.
[8] O.H. Gröhn, M.I. Kettunen, H.I. Mäkelä, M. Penttonen, A. Pitkänen, J.A. Lukkarinen, R.A. Kauppinen, Early detection of irreversible cerebral ischemia in the rat using dispersion of the MRI relaxation time, $T_{1\rho}$, J. Cereb. Blood Flow Metab. 20 (2000) 1457–1466.
[9] J.M. Hakumäki, O.H. Gröhn, K. Tyynelä, P. Valonen, S. Ylä-Herttuala, R.A. Kauppinen, Early gene therapy-induced apoptotic response in BT4C gliomas by magnetic resonance relaxation contrast T_1 in the rotating frame, Cancer Gene Ther. 9 (2002) 338–345.
[10] M.I. Kettunen, A. Sierra, M.J. Närväinen, P.K. Valonen, S. Ylä-Herttuala, R.A. Kauppinen, O.H. Gröhn, Low spin-lock field T_1 relaxation in the rotating frame as a sensitive MR imaging marker for gene therapy treatment response in rat glioma, Radiology 243 (2007) 796–803.
[11] S. Michaeli, G. Oz, D.J. Sorce, M. Garwood, K. Ugurbil, S. Majestic, P. Tuite, Assessment of brain iron and neuronal integrity in patients with Parkinson's disease using novel MRI contrasts, Mov. Disord. 22 (2007) 334–340.
[12] S. Michaeli, H. Gröhn, O. Gröhn, D. Sorce, R. Kauppinen, C. Springer, K. Ugurbil, M. Garwood, Exchange-influenced $T_{2\rho}$ contrast in human brain images measured with adiabatic radio frequency pulses, Magn. Reson. Med. 53 (2005) 823–829.
[13] S. Michaeli, D. Sorce, D. Idiyatullin, K. Ugurbil, M. Garwood, Transverse relaxation in the rotating frame induced by chemical exchange, J. Magn. Reson. 169 (2004) 293–299.
[14] S. Michaeli, D. Sorce, C. Springer, K. Ugurbil, M. Garwood, $T_{1\rho}$ MRI contrast in the human brain: modulation of the longitudinal rotating frame relaxation shutter-speed during an adiabatic RF pulse, J. Magn. Reson. 181 (2006) 138–150.
[15] W.R. Witschey, A. Borthakur, M.A. Elliott, E. Mellon, S. Niyogi, C. Wang, R. Reddy, Compensation for spin-lock artifacts using an off-resonance rotary echo in $T_{1\rho,\mathrm{off}}$-weighted imaging, Magn. Reson. Med. 57 (2007) 2–7.
[16] T. Liimatainen, D.J. Sorce, R. Connell, M. Garwood, S. Michaeli, MRI Contrast from relaxation along a fictitious field (RAFF), Magn. Reson. Med. 64 (2010) 983–994.
[17] A.G. Redfield, Theory of nuclear relaxation processes, Adv. Magn. Reson. 1 (1965) 1–32.
[18] M. Garwood, Y. Ke, Symmetric pulses to induce arbitrary flip angles with compensation for rf inhomogeneity and resonance offsets, J. Magn. Reson. 94 (1991) 511–525.
[19] C. Slichter, Principles of Magnetic Resonance, 3rd ed., Springer Heidelberg, 1996.
[20] C. Griesinger, R.R. Ernst, Cross relaxation in time-dependent nuclear spin system: invariant trajectory approach, Chem. Phys. Lett. 152 (1988) 239–247.
[21] T. Ceckler, J. Maneval, B. Melkowits, Modeling magnetization transfer using a three-pool model and physically meaningful constrains of the fitting parameters, J. Magn. Reson. 151 (2001) 9–27.
[22] J.T. Vaughan, G. Adriany, M. Garwood, E. Yacoub, T. Duong, L. DelaBarre, P. Andersen, K. Ugurbil, Detunable transverse electromagnetic (TEM) volume coil for high-field NMR, Magn. Reson. Med. 47 (2002) 990–1000.
[23] M. Garwood, L. DelaBarre, The return of the frequency sweep: designing adiabatic pulses for contemporary NMR, J. Magn. Reson. 153 (2001) 155–177.
[24] M.H. Levitt, R. Freeman, Compensation for pulse imperfections in NMR spin-echo experiments, J. Magn. Reson. 43 (1981) 65–80.